Transition metal ion FRET to measure short-range distances at the intracellular surface of the plasma membrane

Sharona E. Gordon, Eric N. Senning, Teresa K. Aman, and William N. Zagotta

Department of Physiology and Biophysics, University of Washington, Seattle, WA 98195

Biological membranes are complex assemblies of lipids and proteins that serve as platforms for cell signaling. We have developed a novel method for measuring the structure and dynamics of the membrane based on fluorescence resonance energy transfer (FRET). The method marries four technologies: (1) unroofing cells to isolate and access the cytoplasmic leaflet of the plasma membrane; (2) patch-clamp fluorometry (PCF) to measure currents and fluorescence simultaneously from a membrane patch; (3) a synthetic lipid with a metal-chelating head group to decorate the membrane with metal-binding sites; and (4) transition metal ion FRET (tmFRET) to measure short distances between a fluorescent probe and a transition metal ion on the membrane. We applied this method to measure the density and affinity of native and introduced metal-binding sites in the membrane. These experiments pave the way for measuring structural rearrangements of membrane proteins relative to the membrane.

The Journal of General Physiology

INTRODUCTION

The plasma membrane is a major site of signal detection, transduction, and propagation in cells. Understanding cell signaling dynamics at the plasma membrane requires approaches that can detect changes in membrane architecture over molecular distances (10–100 Å) and biological time scales (milliseconds to seconds). Methods that provide access to dynamics at the intracellular surface of the plasma membrane would be especially powerful. Fluorescence resonance energy transfer (FRET) was first applied to studies of membrane dynamics by Keller et al. (1977), who recognized that fluorescent probes incorporated into membranes could be used as an indicator of mixing of the two membranes during membrane fusion. FRET occurs when the emission spectrum of a donor fluorophore overlaps with the absorption spectrum of an acceptor, and the donor and acceptor are in close proximity (Lakowicz, 2006; Taraska and Zagotta, 2010). FRET is steeply distance dependent, and each donor–acceptor pair has a characteristic distance at which the FRET efficiency is 50% (R_0), where the amount of FRET is optimally sensitive to changes in distance. The R_0 value for fluorescein and rhodamine, for example, is ∼60 Å (Delgadillo and Parkhurst, 2010), making them an ideal FRET pair for quantifying membrane fusion (Keller et al., 1977).

Transition metal ion FRET (tmFRET) is a method to probe the shorter distances typical of the conformational landscape of proteins (Taraska and Zagotta, 2010). tmFRET is a form of FRET that uses a fluorophore as a donor and a nonfluorescent transition metal ion as an acceptor (Latt et al., 1970, 1972; Horrocks et al., 1975; Richmond et al., 2000; Sandtner et al., 2007; Taraska et al., 2009a,b; Yu et al., 2013). Transition metal ions such as Ni^{2+}, Co^{2+}, and Cu^{2+} have broad absorption spectra that overlap the emission spectra of visible light fluorophores (see Miessler and Tarr [1999] pages 361–380 for a discussion of electronic spectra of coordination compounds). Transition metals can therefore accept energy transfer from a nearby donor fluorophore and quench the donor's fluorescence. The degree of quenching is a direct measure of the FRET efficiency (Lakowicz, 2006; Taraska et al., 2009a). The FRET efficiency is steeply dependent on distance between the donor and acceptor, allowing tmFRET to serve as a molecular ruler for distances in the membrane. The main advantages of tmFRET over classical FRET methods are (a) R_0 is very short (∼10–20 Å), allowing short-range interactions to be studied; (b) the transition metals have multiple transition dipoles, reducing the orientation dependence of FRET (Horrocks et al., 1975); (c) the metals can be reversibly bound to native and introduced binding sites; and (d) different metals have different absorption properties, and therefore R_0's, allowing the choice of metal to be tuned to the distance of interest.

Extending tmFRET to studying dynamics in cell membranes would provide a powerful tool for exploring the structure of the membrane (e.g., microdomains), assembly of multiprotein complexes (e.g., scaffolding proteins and their associated proteins), rearrangements

Correspondence to Sharona E. Gordon: seg@uw.edu; or William N. Zagotta: zagotta@uw.edu

Abbreviations used in this paper: FRET, fluorescence resonance energy transfer; PCF, patch-clamp fluorometry; TIRF, total internal reflection fluorescence; tmFRET, transition metal ion FRET.

The Rockefeller University Press $30.00
J. Gen. Physiol. Vol. 147 No. 2 189–200
www.jgp.org/cgi/doi/10.1085/jgp.201511530

in membrane proteins (e.g., ion channels and receptors), and interactions among signaling lipids and membrane proteins (e.g., phosphoinositides and channels/transporters). We have been particularly interested in implementing tmFRET on the cytoplasmic surface of the cell plasma membrane to measure conformational rearrangements of membrane proteins relative to the membrane that occur as part of cell signaling. If a dynamic region of a membrane protein were labeled with a fluorophore and a transition metal were bound to the membrane, tmFRET could be used to report movement of the membrane protein relative to the membrane. Although classical FRET has been used to measure movements of α_4 integrin relative to the membrane, because of the long R_0's of these fluorophores (FITC and rhodamine B), the experiments were only sensitive to distance changes with large separations of the fluorophores (Chigaev et al., 2003).

In this paper, we apply tmFRET to the native membrane. We isolated plasma membrane sheets using both a sonication method and the patch-clamp technique. We show that these plasma membranes contain endogenous, low-affinity binding sites for metals that act as acceptors for tmFRET with a fluorescently labeled lipid in the membrane (Fig. 1). Furthermore, we show that high-affinity metal-binding sites can be introduced to the native membrane at sufficient density to exhibit FRET. This combination of approaches will allow for studies of membrane structure and dynamics that underlie cell signaling.

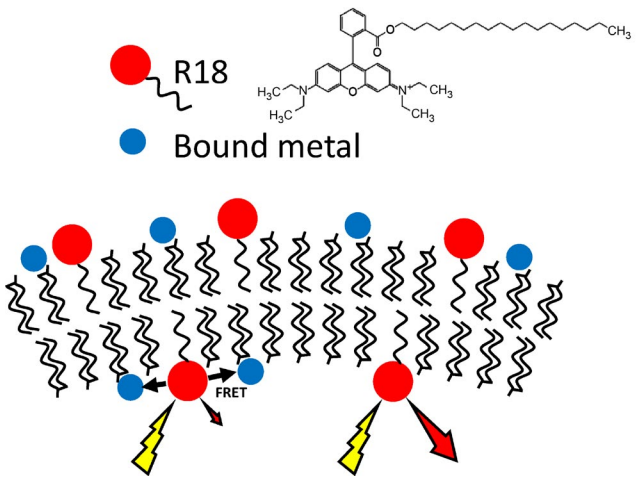

Figure 1. Schematic representation of tmFRET experimental strategy. The membrane-resident dye R18 is depicted by a red sphere atop an acyl chain. Bound transition metal is depicted as a blue sphere. The inset structure is that of R18. If R18 and membrane-bound metal ions are sufficiently close, excitation of R18 (lightning bolt) will excite the donor fluorophore whose emission will be quenched by tmFRET with the acceptor transition metal.

MATERIALS AND METHODS

Cell culture

F-11 cells (gift of M.C. Fishman, Massachusetts General Hospital, Boston, MA; Francel et al., 1987) were cultured at 37°C, 5% CO_2 in Ham's F-12 Nutrient Mixture (#11766064; Gibco) supplemented with 20% fetal bovine serum (#26140-079; Gibco), HAT supplement (100 µM sodium hypoxanthine, 400 nM aminopterin, 16 µM thymidine; #21060-017; Gibco), and penicillin/streptomycin (#15140-122; Gibco). HEK 293T/17 cells (CRL-11268; ATCC) were cultured at 37°C, 5% CO_2 in Dulbecco's modified Eagle's medium (#11995065; Gibco) containing 25 mM glucose, 1 mM sodium pyruvate, and 4 mM L-glutamine. Culture medium was supplemented with 10% fetal bovine serum and penicillin/streptomycin. ND7/23 cells (92090903-1VL; Sigma-Aldrich) were cultured at 37°C, 5% CO_2 in Dulbecco's modified Eagle's medium containing 25 mM glucose, 1 mM sodium pyruvate, and 4 mM L-glutamine. Culture medium was supplemented with 10% heat-inactivated fetal bovine serum and penicillin/streptomycin. Serum heat inactivation was performed by incubating at 56°C for 30 min. PC-12 cells (CRL-1721; ATCC) were cultured at 37°C, 5% CO_2 in Dulbecco's modified Eagle's medium containing 25 mM glucose, 1 mM sodium pyruvate, and 4 mM L-glutamine. Culture medium was supplemented with 5% fetal bovine serum, 5% horse serum (#26050-088; Gibco), and penicillin/streptomycin.

Cell unroofing

We followed an unroofing protocol previously used for electron microscopy (Heuser, 2000) with minor modifications. 24–48 h after cells were passaged onto coverslips (prepared by incubation with filter sterilized 0.12 mg/ml poly-lysine [#P3813; Sigma-Aldrich] in H_2O for 20 min and washed twice with PBS [P3813; Sigma-Aldrich] to remove excess poly-lysine), coverslips were removed from the incubator and placed in our perfusion chamber on the TiE inverted microscope (Nikon) at room temperature. Gentle flow was used to wash with PBS (PBS, 1 pack of P3813 [Sigma-Aldrich]; 2 mM $CaCl_2$ [C5080; Sigma-Aldrich]; 1 mM $MgCl_2$ [5958-04; Mallinckrodt], pH measured at 7.3 and not adjusted; filter sterilized through a 0.22-µm membrane) for 15 min. The sonicator probe (101-148-062, 3-mm tapered tip; Bronson Sonifier) was then positioned in the chamber, with its tip ∼2 mm from the top of the coverslip. Poly-lysine (0.1 mg/ml in PBS; 30,000–70,000 MW; P7886; Sigma-Aldrich) was then perfused through the chamber for 10 s. The poly-lysine treatment caused an expanded cell footprint and improved adherence to the coverslip upon sonication. Swell buffer (a dilution of one part stabilization buffer to two parts water) was then rinsed through the chamber for 30 s, and then stabilization buffer (70 mM KCl [P9333; Sigma-Aldrich], 30 mM HEPES [H4034; Sigma-Aldrich], and 1 mM $MgCl_2$ [5958-04; Mallinckrodt]; initial pH measured at 5.2 and adjusted to 7.4 with KOH; sterile filtered through a 0.22-µm membrane) was used to rinse the chamber well. The vacuum line was then turned off, and the chamber was allowed to fill with as much stabilization buffer as possible without flowing over. A sonic pulse from the probe sonicator (400 W Branson Sonifier) was given for 0.4 s with a power setting of 2. The probe was then removed from the chamber and the experiment commenced.

Membrane labeling with R18 and C18-NTA

Octadecyl rhodamine B (R18; O-246; Life Technologies) was made as a 10-mM stock in EtOH or a 1-mM stock in DMSO and stored at −20°C. For labeling, the stock was freshly diluted for each experiment in the recording solution at the indicated concentration. C18-NTA (N2,N2-bis(carboxymethyl)-N6-(1-oxooctadecyl)-L-lysine) was custom synthesized by Toronto Research Chemicals. It was made as a 10-mM stock in DMSO and stored at −20°C. The C18-NTA

was diluted to 1 µM in stabilization buffer supplemented with 10 µM $CoSO_4$ and applied as described in Results.

Imaging of unroofed cells

Experiments with unroofed cells were performed using a TiE inverted microscope (Nikon) with either a 10× objective (0.3 NA) or a 60× (1.49 NA) oil immersion objective with the Perfect Focus system (Nikon) for preventing focal drift. Excitation for epifluorescence was provided by a xenon lamp (Lambda LS, 175 W; Sutter Instrument) using a filter set for rhodamine B (561-nm/10-nm band-pass excitation filter, 575-nm long-pass emission filter). A total internal reflection fluorescence (TIRF) launch (Nikon) was used to get 561-nm laser excitation for TIRF microscopy experiments. All imaging data were collected with NIS-Elements AR software (Nikon) controlling a QuantEM 512SC camera (Photometrics).

Image analysis was performed with ImageJ (National Institutes of Health; Schneider et al., 2012). Typically, regions of interest were created surrounding individual cells, and nearby regions of interest were created in areas devoid of cells to represent the background. In all cases, the mean gray value of the background region was subtracted from the mean gray value of the cell regions. The fluorescence used to normalize the data were collected in the presence of EDTA to minimize quenching caused by binding of stray metal ions in the water to the NTA head group. Data were analyzed and plotted with Excel 2013 (Microsoft) and Igor Pro (WaveMetrics).

Patch-clamp recording

Inside-out patches were excised from defolliculated *Xenopus laevis* oocytes, as described previously (Zagotta et al., 1989). The pipette (300–700 kΩ) and bath recording solutions each contained either 130 mM NaCl, 3 mM HEPES, and 0.2 mM EDTA, pH 7.2 (epifluorescent patch-clamp fluorometry [PCF]), or 130 mM KCl, 3 mM HEPES, and 0.2 mM EDTA, pH 7.4 (confocal PCF). Patch potential was maintained at 0 mV with either an EPC10 plus amplifier/digitizer and Patchmaster software (HEKA; epifluorescent experiments) or an Axopatch 200B patch-clamp amplifier (Axon Instruments) with an ITC16 interface and Pulse software (HEKA; confocal experiments). Solutions on the patch were changed using a µFlow Perfusion system (ALA Scientific Instruments).

Confocal patch imaging

Confocal microscopy was performed on an LSM 710 microscope (Carl Zeiss) with 40× water immersion lens (1.1 NA) and Zen software (Carl Zeiss). Oocytes were labeled before seal formation with 100 µM fluorescein C5-maleimide (F5M; 62245; Life Technologies) in ND96 solution (96 mM NaCl, 2 mM KCl, 1.8 mM $CaCl_2$, 1 mM $MgCl_2$, and 5 mM HEPES, pH 7.6) for 15 min and then were washed three times with ND96 solution. After patch formation and excision, the patch was perfused with 3 µM R18 in recording solution (130 mM KCl and 3 mM HEPES, pH 7.4; Video 2). For R18, a 561-nm diode laser was used for excitation, and the light was collected from 574 to 625 nm. For F5M, the 488-nm line of an argon laser was used for excitation, and the light was collected from 507 to 541 nm.

Epifluorescent patch imaging

Patches were imaged using an Eclipse TE2000-E microscope (Nikon) with a 60× water immersion objective (1.2 NA) and an Evolve 512 EMCCD camera (Photometrics) and MetaMorph software (Molecular Devices). To label, patches were perfused with 100–250 nM R18 in recording solution (130 mM NaCl, 3 mM HEPES, and 0.2 mM EDTA, pH 7.2) for 1–2 min. To monitor labeling, patches were excited with epifluorescence (Lambda LS with Smart Shutter; Sutter Instrument) and a 560/10-nm excitation filter (Chroma Technology Corp.) and imaged with a 615/60 emission filter (Chroma Technology Corp.) until fluorescence of the patch reached steady state. After labeling, fluorescence of the patch was measured in the presence and absence of 1 µM Co^{2+}. Quenching of fluorescence by Co^{2+} was compared before and after application of Co^{2+}-C18-NTA (1–2.5 µM) for 1 min. Quenching was reversed by washing the patches with 20 mM EDTA for several minutes. To analyze, the mean patch intensity was background subtracted and normalized to the fluorescence in the presence of EDTA to minimize quenching caused by binding of stray metal ions in the water to the NTA head group (MetaMorph software).

Spectrophotometry and spectrofluorometry

Absorption spectra were recorded with a DU 800 spectrophotometer (Beckman Coulter). Fluorescence excitation and emission spectra were recorded with a Fluorolog 3 spectrofluorometer using FluorEssence software (HORIBA Jobin Yvon). For emission spectra, 5.2 nM rhodamine B (R6626; Sigma-Aldrich) in stabilization buffer was placed in a 100-µl chamber of a 0.2-cm by 1-cm quartz cuvette and excited at 550 nm, and the emission spectrum was recorded from 560 to 700 nm. Co^{2+}-NTA was added at concentrations of 0–190 mM from a stock solution of 200 mM $CoSO_4$ (C6768; Sigma-Aldrich) and 300 mM NTA (72560; Sigma-Aldrich) made in stabilization buffer and pH adjusted to 7.4 with KOH. All Co^{2+}-NTA concentrations given refer to the total concentration of Co^{2+}, with the ratio of Co^{2+} to NTA constant at 2:3. To account for the decrease in excitation and emission intensities caused by the optical density of the metal, observed fluorescence intensities of the sample were corrected for the inner filter effect according to the following equation (Lakowicz, 2006):

$$F_{ci} = F_{oi}\left(10^{(0.1*\mathrm{OD}_{550}+0.5*\mathrm{OD}_{i})}\right), \quad (1)$$

where F_{ci} and F_{oi} represent the corrected and observed fluorescence intensities at i-nm wavelength, and OD_{550} and OD_i are the absorption of Co^{2+}-NTA recorded at 550-nm and i-nm wavelength, respectively. Each Co^{2+}-NTA concentration was repeated four times. The FRET efficiency was then calculated using the following equation:

$$\text{FRET efficiency} = 1 - F_{Co} / F, \quad (2)$$

where F and F_{Co} are the corrected fluorescence intensities in the absence and presence of Co^{2+}, respectively.

FRET: Theoretical framework

The theoretical framework for our calculations of tmFRET between a fluorescent donor and transition metal acceptor embedded in a two-dimensional surface is based on the distance dependence of FRET efficiency as described by Förster (1949). We have adopted the modification by Fung and Stryer (1978) of the classical energy transfer equations to calculate the theoretical tmFRET efficiency in our experiments numerically, making the following assumptions: (a) random distribution of the acceptors with respect to donors (in two dimensions or three dimensions; see Eqs. 4 and 5), with a closest approach distance (R_c); (b) no diffusion of the donors and acceptors on the time scale of the lifetime of the donor; and (c) random orientations of the donors and acceptors. The FRET efficiency between randomly positioned donors and acceptors was defined as

$$\text{FRET efficiency} = 1 - \frac{\int_0^\infty e^{(-t/\tau_D)} e^{\left[-\sigma S(t)\right]} dt}{\int_0^\infty e^{(-t/\tau_D)} dt}, \quad (3)$$

where τ_D is the donor fluorescence lifetime, the integral in the denominator is the donor fluorescence in the absence of acceptor, and the integral in the numerator is the donor fluorescence

in the presence of acceptor at some density, σ. The energy transfer term, $e^{[-\sigma S(t)]}$, contains a function $S(t)$ that defines the coupling efficiency. For the three-dimensional case of donors and acceptors in solution (see Fig. 4 C, red curve), the FRET efficiency was calculated with Eq. 3 using the following equation for $S(t)$:

$$S(t) = \int_{R_c}^{\infty} \left\{ 1 - e^{\left[-(t/\tau_D)(R_0/r)^6 \right]} \right\} 4\pi r^2 dr. \quad (4)$$

For the two-dimensional case of donors and acceptors in the membrane (see Fig. 8 B), we used the following equation:

$$S(t) = \int_{R_c}^{\infty} \left\{ 1 - e^{\left[-(t/\tau_D)(R_0/r)^6 \right]} \right\} 2\pi r dr, \quad (5)$$

where r is the distance between donor and acceptor, R_0 is the characteristic distance for the donor and acceptor at which FRET efficiency is 50%, and the integration range is bounded on one side by a closest approach distance, R_c, between donor and acceptor.

We first calculated the expected FRET efficiency between rhodamine B and Co^{2+}-NTA in solution so that we could establish how well the theory approximated tmFRET data in three dimensions. We used MATLAB (MathWorks) to perform numerical calculations of the theoretical FRET efficiency with the bounded integral in Eq. 4 over a volume. R_0 for rhodamine B and Co^{2+}-NTA was calculated as 12.0 Å based on our own emission and absorption spectra of rhodamine B and Co^{2+}-NTA, respectively, in stabilization buffer (see Fig. 4 A) and assuming κ^2 of 2/3 (Fung and Stryer, 1978; Loura, 2012). A fluorescence lifetime, τ_D, of 1.5 ns was used for rhodamine B (see Fig. 4 D; Kristoffersen et al., 2014). We found that R_c at or below 5.0 Å approximated the data well, as determined by eye (see Fig. 4 C). Going below this value of R_c did not bring about a greatly improved fit, and we surmised that, given the structures of rhodamine B and NTA, an R_c of 5.0 Å was reasonable. For the two-dimensional tmFRET model (see Fig. 8 B), we used the R_c value of 5.0 Å determined from fitting the three-dimensional FRET data (Eq. 4). R_c values that are smaller than this seem unlikely in the context of the probes being attached as headgroups onto stearoyl lipids.

Fluorescence lifetime measurements

Fluorescence lifetimes were measured using a FluoTime 100 (PicoQuant) with 470-nm laser excitation with a repetition frequency of 10 MHz and a 60-s integration time. A 1:10 LUDOX solution in water, with transmittance set to 0.1% and no emission filter was used for measuring the instrument response function. 1 µM rhodamine B in stabilization buffer was used, with the instrument set at 100% transmittance and a 490-nm long-pass filter and either no Co^{2+} or 60 mM Co^{2+}-NTA. Lifetime measurements were made in triplicate using three independently prepared samples. Data were analyzed with the DecayFit script (http://www.fluortools.com/software/decayfit) in MATLAB.

Statistics

To determine whether the fluorescence of membranes treated with Co^{2+} differed from those without Co^{2+}, we used paired, two-tailed Student's *t* test assuming unequal variances. For comparing quenching of R18 by Co^{2+} in unroofed cells with that in patches, we used an unpaired, two-tailed Student's *t* test assuming unequal variances. Significance values were set to $P \leq 0.05$.

Online supplemental material

One supplemental figure and two videos are included. Fig. S1 shows the time course of labeling by R18 of an inside-out excised patch from a *Xenopus* oocyte. Video 1 shows a 3-D reconstruction of an R18-labeled patch from a *Xenopus* oocyte. Video 2 shows a time lapse of labeling of an inside-out patch from *Xenopus* oocytes with R18. Online supplemental material is available at http://www.jgp.org/cgi/content/full/jgp.201511530/DC1.

RESULTS

To use tmFRET to study biological membrane structure and dynamics, we needed to introduce a donor fluorophore into the membrane. In contrast to synthetic systems, in which fluorescent phospholipids can be easily incorporated into the lipid mixture used for bilayer formation, we were unable to incorporate fluorescent diacyl dyes, such as diI- and phosphatidylethanolamine-based dyes, into cell membranes efficiently and at high density. Previously, however, the lipophilic cationic fluorescent dye octadecyl rhodamine B (R18) has been shown to label cell membranes (Keller et al., 1977). R18 contains a single acyl chain attached to a highly fluorescent rhodamine B head group (Fig. 1). When added to the aqueous solutions bathing HEK293T/17 cells, R18 efficiently incorporated into the cell's membranes (Fig. 2 B) and is known to remain in cell membranes for >24 h (Keller et al., 1977). Strong plasma membrane staining could also be seen using TIRF microscopy (Fig. 2 B), suggesting that most of the R18 was incorporated into the plasma membrane.

Cell unroofing to access the intracellular surface of the plasma membrane

We next sought a system that would allow us to access the cytosolic surface of the native plasma membrane where many of the membrane signaling events occur. To study the native plasma membrane of a cell, we used the method of unroofing (Heuser, 2000). This method involved positioning a probe sonicator ∼2 mm above adherent cells grown on glass and giving a brief sonic pulse (Fig. 2 A). The result was disruption of the cell plasma membrane that was not adhered to the glass, that is the dorsal surface, and removal of most of the cells contents, leaving only the ventral plasma membrane as a sheet attached to the coverslip. A significant electron microscopy literature using unroofed cells indicates that they are free from most intracellular membranes and other cytosolic constituents and provide access to the cytoplasmic surface of the plasma membrane (Heuser, 2000; Sochacki et al., 2014). An example using HEK293T/17 cells is shown in Fig. 2 C. After fluorescent labeling by R18, the cells were unroofed. Whereas the unroofed cells were barely visible with brightfield microscopy (Fig. 2 C, left), the glass-adhered, R18-stained membranes of the unroofed cells were clearly visible with epi-illumination fluorescence microscopy (Fig. 2 C, middle). The epifluorescence images were virtually indistinguishable from the TIRF

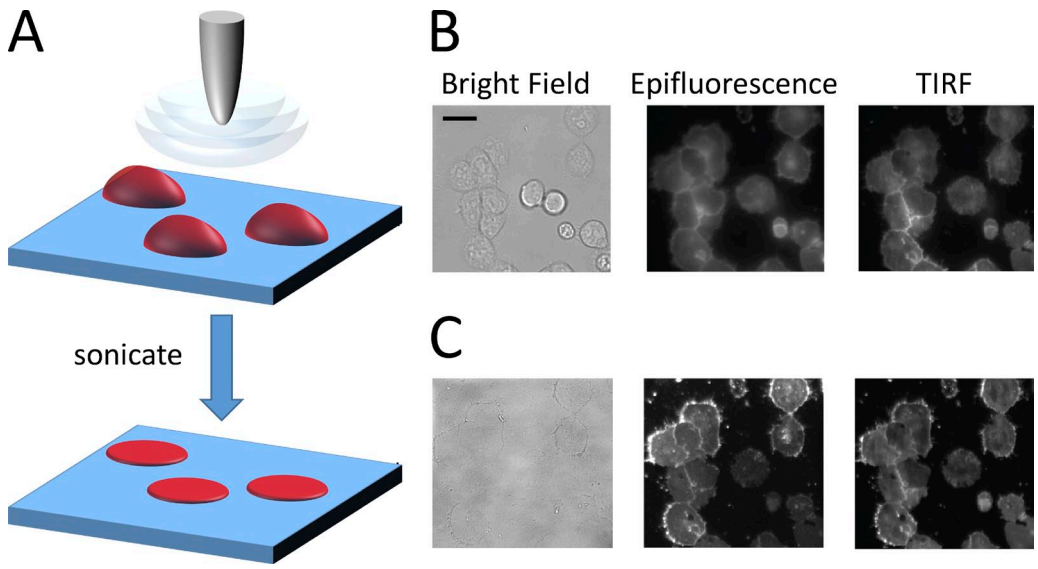

Figure 2. Unroofing adhered cells produces plasma membrane sheets. (A) Cartoon of the unroofing approach. A sonicator probe is shown within 2 mm of R18-labeled, adhered cultured cells. One pulse at low power disrupts the cellular contents, leaving the ventral surface of the cell on the glass. (B and C) Example of unroofing in a field of R18-stained HEK293T/17 cells. Cells before sonication are shown in B, and the same field after unroofing is shown in C. Scale bar applies to all images and is 20 µm.

images (Fig. 2 C, right), suggesting that the R18 label in unroofed cells is almost all within the evanescent field (~200 nm above the glass coverslip). These unroofed cells provided a reduced preparation to study the structure and dynamics at the cytoplasmic leaflet of the plasma membrane.

Unroofing was also effective in other cell types we tried. For these and subsequent experiments, R18 labeling was performed after unroofing (Fig. 3 A). Fig. 3 B shows examples of R18-stained, unroofed cells of various types including HEK293T/17, PC-12, F-11, and ND7/23 cells. For many cells, there was a perimeter of higher fluorescence that may represent an area where the membrane is ruffled or partly folded back on itself. In addition for some cells, especially F-11 cells, there were fine processes that were more brightly labeled, and perhaps not fully unroofed. However, for HEK293T/17 cells and PC-12 cells, examples could easily be found of cells that had relatively uniform staining of the plasma membranes with R18. These unroofed cells proved ideal for developing and optimizing our method for measurements of intramembrane tmFRET.

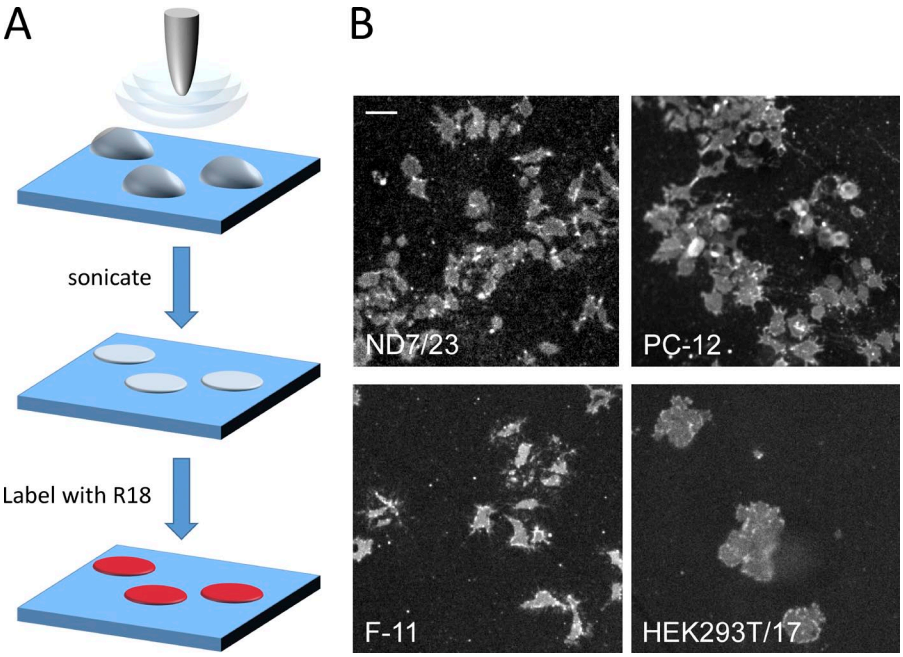

Figure 3. Cell unroofing is useful for a variety of adherent cell types. (A) Cartoon of unroofing approach in which cells are stained with R18 (red) after sonication. (B) Unroofed and stained ND7/23, PC-12, F-11, and HEK293T/17 cells imaged with epifluorescence microscopy. Scale bar applies to all images and is 50 µm.

tmFRET between rhodamine B and Co^{2+}-NTA

R18 is well suited for tmFRET measurements. We measured the emission spectrum of rhodamine B (the fluorescent head group of R18) in solution and found it to overlap with the broad absorption spectra of various transition metals, including Co^{2+} (Fig. 4 A). The absorption spectrum of transition metals can be affected by their chelation state (Reddy, 2010) and is shown in Fig. 4 A for Co^{2+} alone (gray trace) and for Co^{2+} chelated with nitrilotriacetic acid (Co^{2+}-NTA; black trace). The overlap between the emission spectrum of rhodamine B (red trace) and the absorption spectrum of Co^{2+}-NTA together with the quantum yield of rhodamine B (~0.3; Magde et al., 1999), predicts an R_0 of 12.0 Å for mobile randomly oriented donors and acceptors ($\kappa^2 = 2/3$; Fung and Stryer, 1978; Loura, 2012).

An example of tmFRET between rhodamine B and Co^{2+}-NTA in solution is shown in Fig. 4 B. Increasing concentrations of Co^{2+}-NTA caused a decrease in the fluorescence of rhodamine B with little or no change in the shape of the emission spectrum (Fig. 4 B). These emission spectra have been corrected for an inner filter effect (prominent at the highest concentration; see Eq. 1) and suggest a FRET-based mechanism for quenching (Taraska et al., 2009a,b; Yu et al., 2013). The efficiency of energy transfer is simply the fraction of fluorescence quenched upon addition of Co^{2+}-NTA (see Eq. 2). Fig. 4 C shows the dependence of FRET efficiency on the Co^{2+}-NTA concentration, along with a model for solution-based FRET in the limit of no diffusion (Fung and Stryer, 1978; Eqs. 3 and 4). A good fit to the data were produced by a model with an R_0 of 12.0 Å and a distance of closest approach (R_c) of 5 Å. The agreement between the model and the data suggests that most, if not all, of the fluorescence quenching was through a FRET-based mechanism.

To confirm that quenching of rhodamine B by Co^{2+}-NTA was caused by FRET, we used time-correlated single photon counting to measure the fluorescence lifetime of rhodamine B in the absence (Fig. 4 D, red) and presence of Co^{2+}-NTA (Fig. 4 D, blue). 60 mM Co^{2+}-NTA caused a dramatic reduction in fluorescence lifetime (Fig. 4 D). The efficiency of energy transfer calculated from lifetime measurements was not significantly different from the efficiency calculated from steady-state quenching (Fig. 4 E). Because static quenching by Co^{2+}-NTA would not reduce the lifetime of rhodamine B, we can rule out any significant contribution from static quenching to our data (Lakowicz, 2006; Taraska and Zagotta, 2010). In addition, the quenching by transition metals has been shown to exhibit the steep distance and metal dependence predicted for FRET (Latt et al., 1972; Taraska et al., 2009a,b; Yu et al., 2013). Although we cannot rule out a small contribution from other forms of energy transfer, these results are consistent with FRET being the primary mechanism for fluorescence quenching by transition metals.

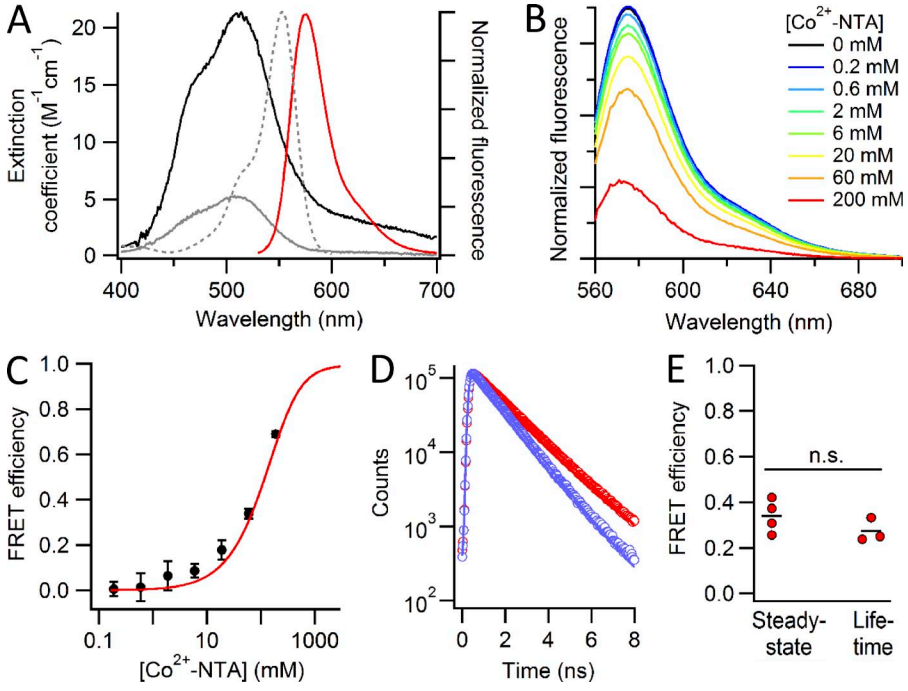

Figure 4. Spectral properties of rhodamine B and Co^{2+} make them ideally suited as a donor and acceptor, respectively, for tmFRET. (A) The absorption spectra of Co^{2+} (gray solid) and Co^{2+}-NTA (black) are shown superimposed on the excitation (gray dashed) and emission (red) spectra of rhodamine B. (B) Emission spectra of rhodamine B fluorescence in solution at the indicated concentrations of Co^{2+}-NTA. (C) Concentration dependence of quenching of rhodamine B in solution by Co^{2+}-NTA (points) fitted with the Fung and Stryer (1978) model (red). The error bars shown represent the SEM of four independent experiments. (D) Fluorescence lifetime measurements of rhodamine B in the absence (red circles) and presence (blue circles) of 60 mM Co^{2+}-NTA. Best fits to the data with a single exponential give time constants of 1.55 ns and 1.18 ns without and with Co^{2+}-NTA, respectively. (E) Energy transfer efficiencies estimated with steady-state and lifetime fluorescence measurements. The mean for each group is shown by the black line. The label n.s. indicates there was no statistically significant difference between the groups ($P > 0.05$).

tmFRET with endogenous metal-binding sites on the membrane

To determine whether there are endogenous metal-binding sites on the membrane, we measured tmFRET in R18-labeled, unroofed PC-12 cells. The addition of 1 mM Co^{2+} caused a dramatic reduction in R18 fluorescence ($F_{Co}/F = 51 \pm 7\%$; $n = 3$), which was readily reversed by the addition of 10 mM EDTA (Fig. 5 A). The quenching was significantly greater than the solution quenching of rhodamine B by 2 mM Co^{2+} (not depicted) or Co^{2+}-NTA in solution (Fig. 4 B), indicating that Co^{2+} was binding to the membrane at a site near R18. The Co^{2+} concentration dependence of quenching was shallow, with a half-maximal quenching concentration of ~40 µM and a Hill slope of 0.53 (Fig. 5 B). These data suggest that the membrane contains multiple types of metal-binding sites with different affinities ranging from micromolar to millimolar. Although the lower affinity sites are present at sufficient density for bound Co^{2+} to exhibit FRET with R18, Co^{2+} at millimolar concentrations likely binds to heterogeneous sites on the membrane and membrane proteins, making structural interpretations of tmFRET difficult.

tmFRET with metal-binding sites introduced into the membrane

To use tmFRET to measure the structure and dynamics of fluorescently labeled elements in the cell membrane, we needed to introduce homogeneous, high-affinity metal-binding sites at a high density in the membrane. For this purpose, we designed a fatty acid with a metal-binding head group, C18-NTA. C18-NTA has the same acyl chain as R18, but with an NTA head group for high-affinity metal binding. Like R18, C18-NTA could be added to aqueous solutions where it would incorporate readily into the plasma membrane of both intact and unroofed cells.

The addition of C18-NTA to unroofed cells caused a dramatic increase in the Co^{2+} binding affinity of the membrane. Fig. 6 A shows the effect of Co^{2+} on a field of unroofed, R18-labeled PC-12 cells before and after treatment with 1 µM C18-NTA for 10 min. After C18-NTA, even 1 µM Co^{2+} produced significant quenching of R18. The quenching by Co^{2+} could be completely reversed by the addition of 10 mM EDTA (Fig. 6 A). The concentration dependence of quenching by Co^{2+} shows that C18-NTA introduced a submicromolar affinity Co^{2+}-binding site (estimated K_d of ~18 nM under our conditions [Anderegg, 1982]) to the membrane that is much higher affinity than the endogenous binding sites (Fig. 6 B; data from same coverslip shown in Fig. 6 A). Therefore, for the remaining experiments, we used 1 µM Co^{2+}, which should saturate the introduced C18-NTA–binding sites, displacing any contaminating metals in our preparations, but not bind appreciably to the endogenous metal-binding sites in the membrane.

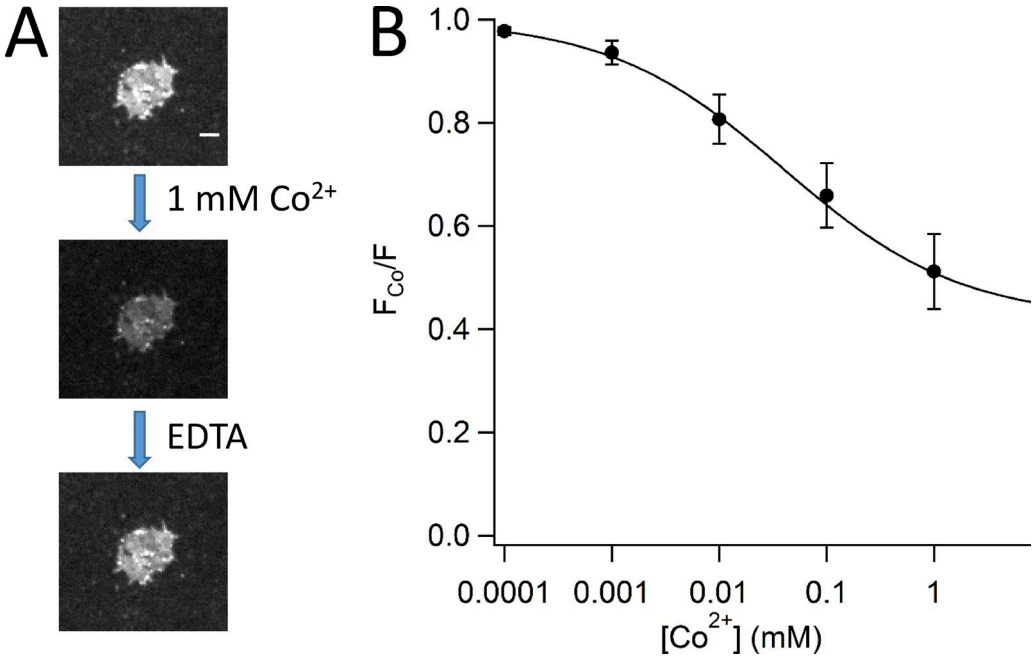

Figure 5. Quenching of R18 in unroofed PC-12 cells by Co^{2+} binding to endogenous metal-binding sites. (A) Exemplar epifluorescent images of unroofed, R18-labeled cells initially (top), in the presence of 1 mM Co^{2+} (middle), and after subsequent washing with EDTA (bottom). Scale bar in top image applies to all images and is 20 µm. (B) Compiled data from exposing many unroofed, R18-labled cells to various concentrations of Co^{2+} in the bath. All cells from eight independent fields were averaged together, and the means from eight fields were then averaged to produce the points and SEM shown. The smooth curve is a fit with the Hill equation, with a $K_{1/2}$ of 40 µM and a slope of −0.53. We did not apply Co^{2+} concentrations >1 mM and allowed the F_{Co}/F value at high concentrations to float during the fit, giving a value of 0.42.

Across cells in all fields examined, application of 1 µM Co^{2+} after C18-NTA treatment produced quenching of the R18 fluorescence, $1 - F_{Co}/F$, of 58 ± 1.6% (n = 35; Fig. 7). This effect was highly variable but significantly larger than the effect 1 µM Co^{2+} had on the fluorescence of cells not pretreated with C18-NTA (F_{Co}/F = 96 ± 1%; n = 35; Fig. 7). The variability was much larger from coverslip to coverslip than from cell to cell in the same coverslip, suggesting variability in the amount of C18-NTA incorporated. Similarly, the degree of quenching of the endogenous metal-binding sites by higher concentrations of Co^{2+} was quite variable (not depicted). Overall, these results indicate that C18-NTA is incorporating high-affinity, reversible metal-binding sites in the membrane at sufficient density for the bound metal to exhibit FRET with R18.

To estimate the density of C18-NTA in the membrane, we fit the metal quenching data to a model based on FRET in two dimensions (Fung and Stryer, 1978). The model assumes random arrangement of donors and acceptors in the membrane and a closest approach distance for the donor and acceptor (Fig. 8 A). The distance of closest approach is the minimum possible distance between the donor and acceptor transition dipoles in two dimensions. Fig. 8 B shows predictions of the model for the FRET efficiency as a function of the acceptor density and the mole fraction of the acceptor, assuming an R_0 of 12.0 Å and a closest approach distance R_e of 5 Å (estimated from solution quenching experiments; Fig. 4 C). From this model, we estimate that the range in the densities of C18-NTA in the membrane is ~0.0017 to 0.0025 C18-NTA molecules per square angstrom of membrane (encompassing the 25th to 75th percentile of the data), corresponding to a mole fraction of between 0.12 and 0.18, assuming a cross-sectional surface area of 70 $Å^2$ per lipid (Fig. 8; Fung and Stryer, 1978).

tmFRET in excised membrane patches

A powerful alternative to unroofing for studying the isolated plasma membrane of cells is the patch-clamp technique (Hamill et al., 1981). Excised inside-out patches provide a cell-free patch of plasma membrane with solution access to the cytoplasmic side of the membrane. In addition, the electronics of the patch-clamp amplifier provide the ability to control the membrane voltage and record ionic currents. PCF allows for fluorescence measurements of structure and dynamics simultaneous with current measurements of function of ion channels and transporters (Zheng and Zagotta, 2000, 2003). This method has been used to measure ligand binding and conformational changes in ion channels (Zheng and Zagotta, 2000; Zheng et al., 2003; Trudeau and Zagotta, 2004; Islas and Zagotta, 2006; Biskup et al., 2007; Taraska and Zagotta, 2007; Kusch et al., 2010; Miranda

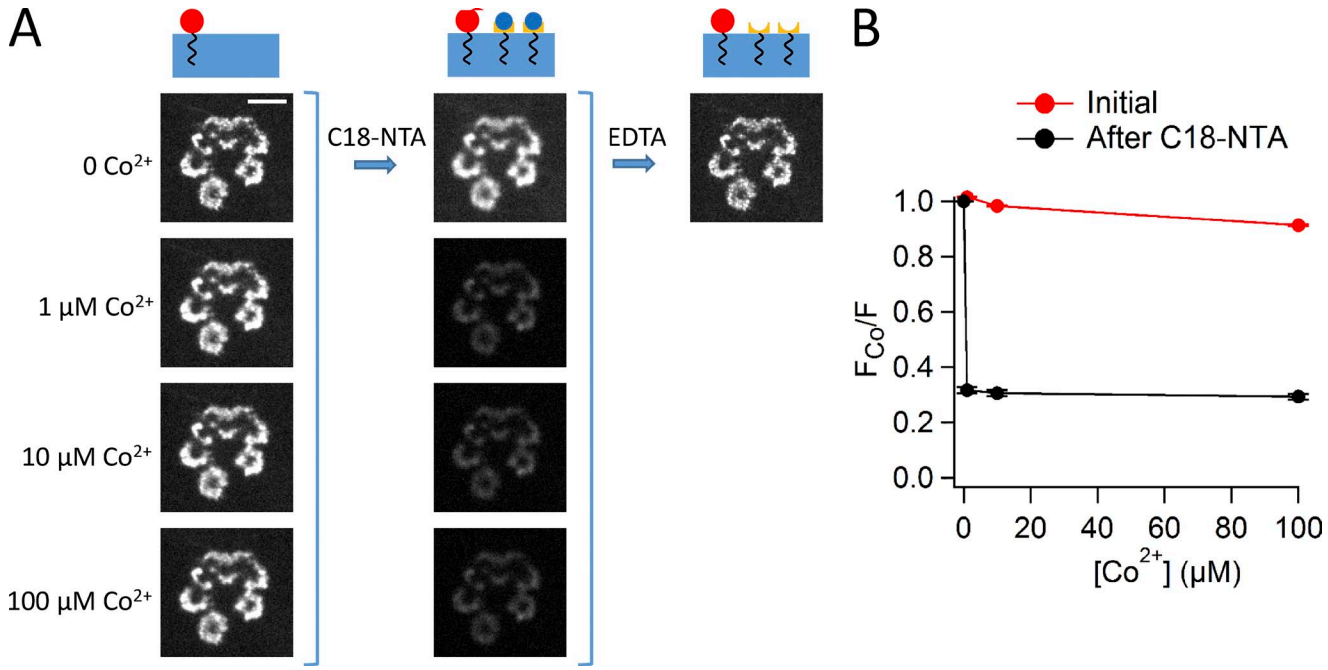

Figure 6. C18-NTA adds high-affinity Co^{2+}-binding sites to unroofed cells. (A) Epifluorescent images represent a field of unroofed, R18-labeled PC-12 cells, with the left-hand column showing the initial fluorescence intensity from 0 to 100 µM Co^{2+} in the bath, as indicated. The unroofed cells were then treated with C18-NTA (see Materials and methods), the C18-NTA was removed from the bath, and cells were then washed with EDTA and then again bathed in 0–100 µM Co^{2+} (middle column). Finally, the unroofed cells were washed with EDTA to recover the fluorescence intensity (right column). Scale bar shown in the top left image applies to all images and is 50 µm. (B) Concentration dependence for coverslip from which the example in A is shown. Points shown are means of the cells, and the bars represent the SEM.

et al., 2013; Kusch and Zifarelli, 2014) and would provide a useful platform for measuring membrane structure and dynamics.

To use PCF to measure tmFRET with the membrane, we have incorporated R18 into membrane patches (Fig. 9). Giant patches from *Xenopus* oocytes were excised in the inside-out configuration and subsequently labeled by exposing the patch to R18 in the bath solution. The oocytes were first labeled with a cysteine-reactive green fluorophore (fluorescein C-5 maleimide, F5M), which labeled cysteine-containing membrane proteins, to allow us to focus on the patch using confocal microscopy (Fig. 9 B). After excision of inside-out patches, the patches were exposed to 3 µM R18 and viewed with confocal microscopy (Fig. 9 C). A three-dimensional reconstruction of the patch shows R18 fluorescence in the patch, on the inner surface of the electrode leading to the patch, and on the tip of the electrode (Video 1). Interestingly, the time course of R18 incorporation showed that the R18 incorporated initially into the membrane at the tip of the patch pipette and subsequently labeled the patch membrane further back in the electrode more slowly, either by diffusion or direct incorporation (Fig. S1 and Video 2). These experiments establish PCF as an effective way to label the isolated plasma membrane.

We next tested whether transition metal-binding sites could be introduced into membrane patches for tmFRET. In the absence of exogenous metal-binding sites, 1 µM Co^{2+} had virtually no effect on the R18 fluorescence in the patch measured with epifluorescence microscopy (Fig. 10, A and B), as we observed in unroofed cells.

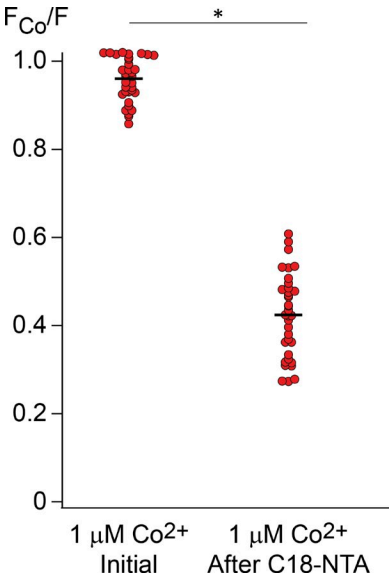

Figure 7. Collected data for quenching of R18 by Co^{2+} before and after treatment of cells with C18-NTA. Each point was measured as the fluorescence from a single unroofed cell, with mean fluorescence from a nearby background region subtracted. The black lines indicate the mean of the data for each condition. Asterisk indicates significance at $P < 0.01$.

However, after the exposure of the patch to 1–2.5 µM C18-NTA, R18 fluorescence was considerably reduced ($F_{Co}/F = 0.68 \pm 0.07$; $n = 4$), indicating significant incorporation of C18-NTA and tmFRET with R18 in the membrane (Fig. 10). The fluorescence quenching was less than we observed in unroofed cells ($P < 0.05$), suggesting either incorporation of less C18-NTA in patches or binding of Co^{2+} to only the intracellular side of the membrane in inside-out patches (see Discussion). The quenching was largely reversed by the addition of 20 mM EDTA (Fig. 10 A). These experiments lay the groundwork for exploring the dynamics of membrane proteins relative to the membrane using tmFRET and PCF.

DISCUSSION

In this paper, we describe a new method for measuring short-range distances at the intracellular leaflet of the plasma membrane. The method involves measuring tmFRET between donor fluorophores attached to

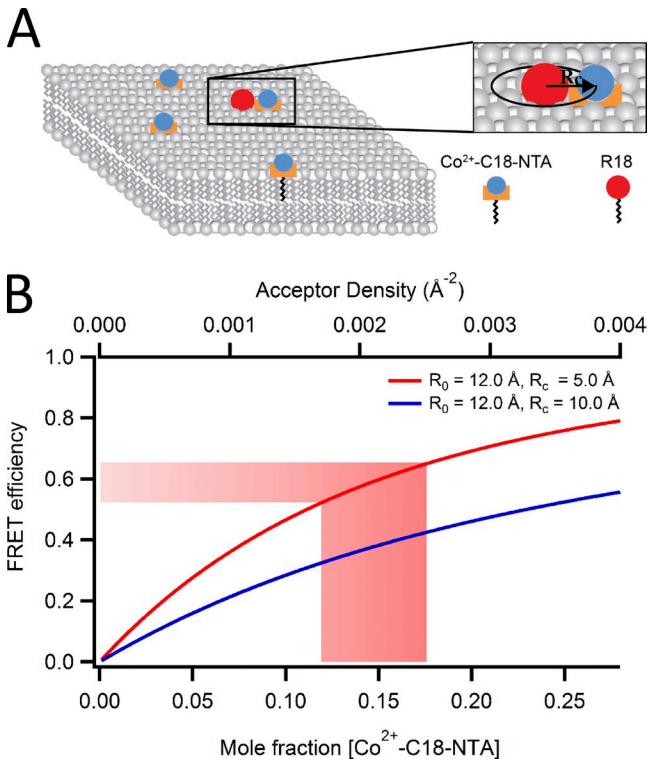

Figure 8. Model for determining Co^{2+} density on the plasma membrane of unroofed cells from its quenching of R18. (A) Cartoon depicting the concept of R_c, the distance of closest approach between the donor (head group of R18) and acceptor (Co^{2+} bound to head group of C18-NTA). (B) Relationship between mole fraction Co^{2+}-bound C18-NTA and FRET efficiency as measured from quenching of R18. For convenience, an axis is also shown for acceptor density. Predictions from the Fung and Stryer (1978) model are shown for an R_c of 5 Å (red) and 10 Å (blue). The red region shows how the 25–75th percentile of the FRET efficiencies, calculated from the data in Fig. 7 using Eq. 2, translates into mole fraction of Co^{2+}-C18-NTA.

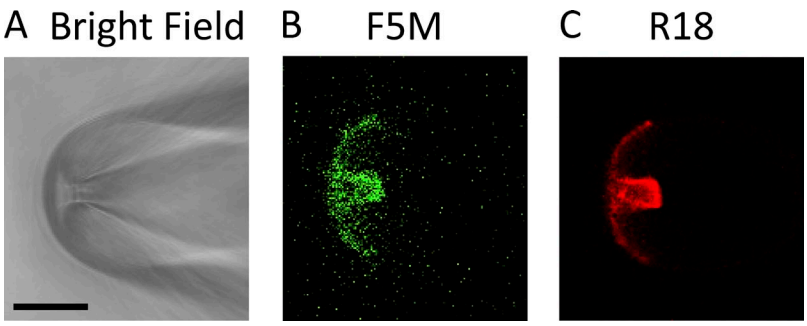

Figure 9. Confocal images of an inside-out excised patch from a *Xenopus* oocyte. (A) Bright-field image of the pipette. Scale bar is 20 µm and also applies to B and C. (B) Fluorescence caused by F5M. (C) Fluorescence caused by R18.

components of the membrane and acceptor transition metal ions bound to metal-binding sites on the membrane. We show that the method works for rhodamine B attached to a fatty acyl tail (R18) in the membrane and Co^{2+} bound to either endogenous metal-binding sites on the membrane or exogenous metal-binding sites on C18-NTA incorporated in the membrane. Furthermore, we show that the tmFRET method can be applied to the intracellular leaflet of the plasma membrane by either unroofing the cells or using the excised inside-out configuration of the patch-clamp technique.

Our approach has several advantages over other FRET methods for measuring the structure and dynamics of the membrane. The measurements are made in native cell membrane without the need to isolate and purify any components or reconstitute in synthetic membranes. The absolute FRET efficiency can be easily determined by simply measuring the reduction in donor fluorescence upon addition of the metal. Because the FRET efficiency is measured from the donor, and the acceptor is nonfluorescent, the metal can be present in molar excess without loss of signal or increased background. Because the extinction coefficients of the metals are small (relative to most fluorophores) the characteristic distance range for tmFRET (R_0) is short and the distance dependence is steep, making it sensitive to the short distances and distance changes found for the molecular interactions occurring in biological membranes. Furthermore, different metals have different absorption properties so the choice of metal ion can be tuned to the particular distance range desired. Finally, unroofing and PCF provide access to the intracellular leaflet of the membrane. Unroofing is potentially amenable to medium- or high-throughput analysis, whereas PCF allows precise control of the membrane voltage and the ability to measure membrane currents.

The amount of tmFRET is sensitive to both the density of the acceptor sites and the distance of closest approach of the donor to the acceptor (R_c) but is insensitive to the density of the donor fluorophore. This allows one to measure either the density of metal-binding sites in the membrane or the distance of closest approach of the metal to the donor fluorophore. If the metal is bound to a component that is enriched in certain regions or microdomains of the membrane, the tmFRET would be expected to be greater in those regions. Here we found that there are endogenous metal-binding sites on the membrane with micromolar to millimolar affinity. These sites

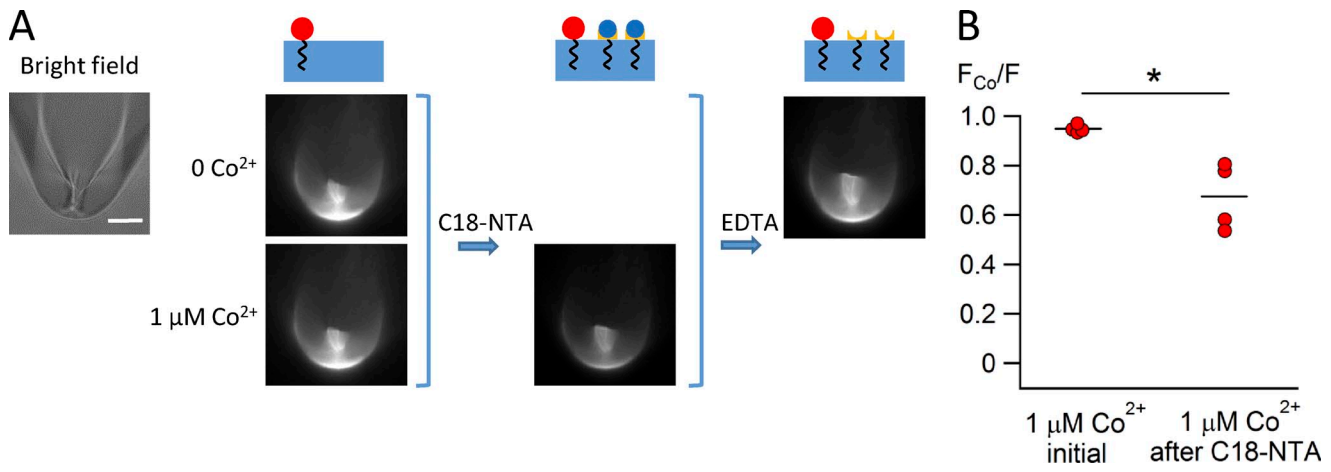

Figure 10. tmFRET between R18 and Co^{2+}-C18-NTA in inside-out patches from a *Xenopus* oocyte. (A) Bright-field and epifluorescence images from a representative patch. Fluorescence images from patches with either 0 or 1 µM Co^{2+} before (left) or after (middle) application of C18-NTA and after 20 mM EDTA (right). Scale bar in top left image applies to all images and is 20 µm. (B) Patch fluorescence in Co^{2+} was normalized to patch fluorescence in EDTA before and after C18-NTA ($n = 4$). Mean (lines) and individual (points) patch values are shown. Asterisk indicates significance at $P < 0.05$.

likely arise from a combination of acidic phospholipids, such as phosphatidylserine and phosphatidylinositides, and membrane proteins. Addition of C18-NTA, however, introduced a high density of high-affinity (submicromolar) metal-binding sites. The degree of quenching was somewhat variable from cell to cell, and the estimated density of introduced metal-binding sites (mole fraction of ∼0.12–0.18) is dependent on assumptions made about the label's flexibility, uniformity, and closest approach distance. If the bound metal ions are not uniformly distributed or in microdomains, the observed FRET efficiency may be a weighted average of the efficiencies in different regions of the membrane. At the current resolution, it is difficult to determine the uniformity of the density within a given cell.

We designed the C18-NTA metal-binding fatty acid to have the same, saturated acyl chain as R18. Although we have not investigated whether the plasma membranes of the cells we studied may be composed of multiple, nonmiscible compartments (e.g., lipid rafts [Simons and Ikonen, 1997]), the residence of a fatty acid within any given compartment should be controlled primarily by the properties of its acyl chain. Therefore, C18-NTA and R18 are expected to reside within the same compartment. Because we determined R_e and the acceptor density empirically, compartmentalization would not invalidate our conclusions. However, if significant compartmentalization is present, it should be noted that the values calculated represent R_e and acceptor density only in the compartment in which the two probes are present.

In the case of fluorescently labeled lipids, one must consider the possibility of transfer of the lipid from one leaflet to the other. This is the case for R18, which equilibrates between the leaflets of the membrane in seconds (Melikyan et al., 1996). In our experiments, the metal may not be bound equally on both leaflets. For example, in the PCF experiments, the metal is applied to only the intracellular face of the membrane and is not expected to access the extracellular side. In this case, the measured FRET efficiency will be averaged between the two leaflets. This may explain the somewhat smaller quenching we observed in our PCF experiments compared with the unroofing experiments. Transfer between leaflets of the bilayer is not expected to be an issue for fluorescently labeled proteins.

If the donor is present on an intracellular domain of a membrane protein, the distance of closest approach will be determined, in part, by the distance of the donor from the membrane. Therefore, movements of the domain closer to the membrane would be expected to increase the amount of tmFRET. For example, a movement of the fluorophore by 5 Å (from 10 Å to 5 Å) would be expected to increase the FRET efficiency by ∼20% (Fig. 8 B). Many membrane proteins, such as ion channels, transporters, and receptors, undergo significant conformational changes during the processes of transport and regulation. These processes have been difficult to study in intact biological membranes because of the need to specifically label the protein and membrane. The method described here provides a way to specifically label the membrane with a nonfluorescent FRET acceptor. Once the protein can be specifically labeled with a donor fluorophore, tmFRET can be used to measure the dynamics of protein movement relative to the membrane (see Zagotta et al. in this issue). Such studies may bridge the gap between the static structures of membrane proteins in crystals and detergent to the dynamic structures of proteins in their native membrane.

We thank Dr. Mark C. Fishman for the gift of the F-11 cells. We thank Stacey Camp and Mika Munari for expert technical assistance.

Research reported in this publication was supported by the National Eye Institute of the National Institutes of Health (NIH) under award numbers R01EY017564 (to S.E. Gordon) and R01EY010329 (to W.N. Zagotta), by the National Institute of Mental Health under award number R01MH102378 (to W.N. Zagotta), by the National Institute of General Medical Sciences of the NIH under award number R01GM100718 (to S.E. Gordon and W.N. Zagotta), by the National Institute of Neurological Disease and Stroke under award number F32NS077622 (to T.K. Aman), by the National Heart Lung Blood Institute of the NIH under award number T32HL007312 (to E.N. Senning), by the American Heart Association under award number 14IRG18770000 (to W.N. Zagotta), and by the following additional awards from NIH: S10RR025429, P30DK017047, and P30EY001730.

The authors declare no competing financial interests.

H. Peter Larsson served as guest editor.

Submitted: 14 October 2015
Accepted: 21 December 2015

REFERENCES

Anderegg, G. 1982. Critical survey of stability constants of NTA complexes: Critical evaluation of equilibrium constants in solution part A: Stability constants of metal complexes. *Pure Appl. Chem.* 54:2693–2758. http://dx.doi.org/10.1351/pac198254122693

Biskup, C., J. Kusch, E. Schulz, V. Nache, F. Schwede, F. Lehmann, V. Hagen, and K. Benndorf. 2007. Relating ligand binding to activation gating in CNGA2 channels. *Nature.* 446:440–443. http://dx.doi.org/10.1038/nature05596

Chigaev, A., T. Buranda, D.C. Dwyer, E.R. Prossnitz, and L.A. Sklar. 2003. FRET detection of cellular α4-integrin conformational activation. *Biophys. J.* 85:3951–3962. http://dx.doi.org/10.1016/S0006-3495(03)74809-7

Delgadillo, R.F., and L.J. Parkhurst. 2010. Spectroscopic properties of fluorescein and rhodamine dyes attached to DNA. *Photochem. Photobiol.* 86:261–272. http://dx.doi.org/10.1111/j.1751-1097.2009.00663.x

Förster, T. 1949. Experimentelle Und Theoretische Untersuchung Des Zwischenmolekularen Ubergangs Von Elektronenanregungsenergie. *Z. Naturforsch. A.* 4:321–327.

Francel, P.C., K. Harris, M. Smith, M.C. Fishman, G. Dawson, and R.J. Miller. 1987. Neurochemical characteristics of a novel dorsal root ganglion X neuroblastoma hybrid cell line, F-11. *J. Neurochem.* 48:1624–1631. http://dx.doi.org/10.1111/j.1471-4159.1987.tb05711.x

Fung, B.K., and L. Stryer. 1978. Surface density determination in membranes by fluorescence energy transfer. *Biochemistry.* 17:5241–5248. http://dx.doi.org/10.1021/bi00617a025

Hamill, O.P., A. Marty, E. Neher, B. Sakmann, and F.J. Sigworth. 1981. Improved patch-clamp techniques for high-resolution current recording from cells and cell-free membrane patches. *Pflugers Arch.* 391:85–100. http://dx.doi.org/10.1007/BF00656997

Heuser, J. 2000. The production of 'cell cortices' for light and electron microscopy. *Traffic.* 1:545–552. http://dx.doi.org/10.1034/j.1600-0854.2000.010704.x

Horrocks, W.D. Jr., B. Holmquist, and B.L. Vallee. 1975. Energy transfer between terbium (III) and cobalt (II) in thermolysin: a new class of metal–metal distance probes. *Proc. Natl. Acad. Sci. USA.* 72:4764–4768. http://dx.doi.org/10.1073/pnas.72.12.4764

Islas, L.D., and W.N. Zagotta. 2006. Short-range molecular rearrangements in ion channels detected by tryptophan quenching of bimane fluorescence. *J. Gen. Physiol.* 128:337–346. http://dx.doi.org/10.1085/jgp.200609556

Keller, P.M., S. Person, and W. Snipes. 1977. A fluorescence enhancement assay of cell fusion. *J. Cell Sci.* 28:167–177.

Kristoffersen, A.S., S.R. Erga, B. Hamre, and Ø. Frette. 2014. Testing fluorescence lifetime standards using two-photon excitation and time-domain instrumentation: rhodamine B, coumarin 6 and lucifer yellow. *J. Fluoresc.* 24:1015–1024. http://dx.doi.org/10.1007/s10895-014-1368-1

Kusch, J., and G. Zifarelli. 2014. Patch-clamp fluorometry: electrophysiology meets fluorescence. *Biophys. J.* 106:1250–1257. http://dx.doi.org/10.1016/j.bpj.2014.02.006

Kusch, J., C. Biskup, S. Thon, E. Schulz, V. Nache, T. Zimmer, F. Schwede, and K. Benndorf. 2010. Interdependence of receptor activation and ligand binding in HCN2 pacemaker channels. *Neuron.* 67:75–85. http://dx.doi.org/10.1016/j.neuron.2010.05.022

Lakowicz, J.R., editor. 2006. Principles of Fluorescence Spectroscopy. Third edition. Springer, New York. 954 pp.

Latt, S.A., D.S. Auld, and B.L. Valee. 1970. Surveyor substrates: energy-transfer gauges of active center topography during catalysis. *Proc. Natl. Acad. Sci. USA.* 67:1383–1389. http://dx.doi.org/10.1073/pnas.67.3.1383

Latt, S.A., D.S. Auld, and B.L. Vallee. 1972. Distance measurements at the active site of carboxypeptidase A during catalysis. *Biochemistry.* 11:3015–3022. http://dx.doi.org/10.1021/bi00766a013

Loura, L.M. 2012. Simple estimation of Förster resonance energy transfer (FRET) orientation factor distribution in membranes. *Int. J. Mol. Sci.* 13:15252–15270. http://dx.doi.org/10.3390/ijms131115252

Magde, D., G.E. Rojoas, and P.G. Seybold. 1999. Solvent dependence of fluorescence lifetimes of xanthene dyes. *Photochem. Photobiol.* 70:737–744. http://dx.doi.org/10.1111/j.1751-1097.1999.tb08277.x

Melikyan, G.B., B.N. Deriy, D.C. Ok, and F.S. Cohen. 1996. Voltage-dependent translocation of R18 and DiI across lipid bilayers leads to fluorescence changes. *Biophys. J.* 71:2680–2691. http://dx.doi.org/10.1016/S0006-3495(96)79459-6

Miessler, G.L., and D.A. Tarr. 1999. Inorganic Chemistry. Second edition. Prentice Hall, Upper Saddle River, NJ. 642 pp.

Miranda, P., J.E. Contreras, A.J. Plested, F.J. Sigworth, M. Holmgren, and T. Giraldez. 2013. State-dependent FRET reports calcium- and voltage-dependent gating-ring motions in BK channels. *Proc. Natl. Acad. Sci. USA.* 110:5217–5222. http://dx.doi.org/10.1073/pnas.1219611110

Reddy, K.V. 2010. Symmetry and Spectroscopy of Molecules. Second edition. New Age Science, Tunbridge Wells, England, UK. 631 pp.

Richmond, T.A., T.T. Takahashi, R. Shimkhada, and J. Bernsdorf. 2000. Engineered metal binding sites on green fluorescence protein. *Biochem. Biophys. Res. Commun.* 268:462–465. http://dx.doi.org/10.1006/bbrc.1999.1244

Sandtner, W., F. Bezanilla, and A.M. Correa. 2007. In vivo measurement of intramolecular distances using genetically encoded reporters. *Biophys. J.* 93:L45–L47. http://dx.doi.org/10.1529/biophysj.107.119073

Schneider, C.A., W.S. Rasband, and K.W. Eliceiri. 2012. NIH Image to ImageJ: 25 years of image analysis. *Nat. Methods.* 9:671–675. http://dx.doi.org/10.1038/nmeth.2089

Simons, K., and E. Ikonen. 1997. Functional rafts in cell membranes. *Nature.* 387:569–572. http://dx.doi.org/10.1038/42408

Sochacki, K.A., G. Shtengel, S.B. van Engelenburg, H.F. Hess, and J.W. Taraska. 2014. Correlative super-resolution fluorescence and metal-replica transmission electron microscopy. *Nat. Methods.* 11:305–308. http://dx.doi.org/10.1038/nmeth.2816

Taraska, J.W., and W.N. Zagotta. 2007. Structural dynamics in the gating ring of cyclic nucleotide-gated ion channels. *Nat. Struct. Mol. Biol.* 14:854–860. http://dx.doi.org/10.1038/nsmb1281

Taraska, J.W., and W.N. Zagotta. 2010. Fluorescence applications in molecular neurobiology. *Neuron.* 66:170–189. http://dx.doi.org/10.1016/j.neuron.2010.02.002

Taraska, J.W., M.C. Puljung, N.B. Olivier, G.E. Flynn, and W.N. Zagotta. 2009a. Mapping the structure and conformational movements of proteins with transition metal ion FRET. *Nat. Methods.* 6:532–537. http://dx.doi.org/10.1038/nmeth.1341

Taraska, J.W., M.C. Puljung, and W.N. Zagotta. 2009b. Short-distance probes for protein backbone structure based on energy transfer between bimane and transition metal ions. *Proc. Natl. Acad. Sci. USA.* 106:16227–16232. http://dx.doi.org/10.1073/pnas.0905207106

Trudeau, M.C., and W.N. Zagotta. 2004. Dynamics of Ca^{2+}-calmodulin-dependent inhibition of rod cyclic nucleotide-gated channels measured by patch-clamp fluorometry. *J. Gen. Physiol.* 124:211–223. http://dx.doi.org/10.1085/jgp.200409101

Yu, X., X. Wu, G.A. Bermejo, B.R. Brooks, and J.W. Taraska. 2013. Accurate high-throughput structure mapping and prediction with transition metal ion FRET. *Structure.* 21:9–19. http://dx.doi.org/10.1016/j.str.2012.11.013

Zagotta, W.N., T. Hoshi, and R.W. Aldrich. 1989. Gating of single Shaker potassium channels in *Drosophila* muscle and in *Xenopus* oocytes injected with Shaker mRNA. *Proc. Natl. Acad. Sci. USA.* 86:7243–7247. http://dx.doi.org/10.1073/pnas.86.18.7243

Zagotta, W.N., M.T. Gordon, E.N. Senning, M. Munari, and S.E. Gordon. 2016. Measuring distances between TRPV1 and the plasma membrane using a noncanonical amino acid and transition metal ion FRET. *J. Gen. Physiol.*. http://dx.doi.org/1085/jgp.201511531

Zheng, J., and W.N. Zagotta. 2000. Gating rearrangements in cyclic nucleotide-gated channels revealed by patch-clamp fluorometry. *Neuron.* 28:369–374. http://dx.doi.org/10.1016/S0896-6273(00)00117-3

Zheng, J., and W.N. Zagotta. 2003. Patch-clamp fluorometry recording of conformational rearrangements of ion channels. *Sci. STKE.* http://dx.doi.org/10.1126/stke.2003.176.pl7

Zheng, J., M.D. Varnum, and W.N. Zagotta. 2003. Disruption of an intersubunit interaction underlies Ca^{2+}-calmodulin modulation of cyclic nucleotide-gated channels. *J. Neurosci.* 23:8167–8175.